Radiation from Hypervelocity Impact Generated Plasma

B. JEAN AND T. L. ROLLINS*
Computing Devices of Canada Ltd., Ottawa, Ontario, Canada

Visible light, referred to as the "impact flash," is radiated during hypervelocity impact. Time-resolved experimental observations of impact flash have been made in a low-vacuum ballistic range. The measurements revealed that the impact flash phenomenon consists of two successive events of distinct origin. The first event is a submicrosecond pulse which time-integrated spectra show to be associated with continuum radiation and with high-density, strongly ionized radiating gas at the point of impact. The second event is a slow-rising, long duration light pulse spectroscopically characterized by line emission of neutral atoms. It was found that this phenomenon was caused by a radially expanding jet of debris whose origin has been theoretically predicted. The investigation showed that measured characteristics of the first event could be related empirically to the size and the velocity of the impacting projectile.

I. Introduction

THE impact of a projectile on a target at hypervelocity has been observed to generate an intense short duration flash of visible radiation at the instant of impact. The phenomenon has received much attention by many authors in order to assess its possible use as an impact signature.[1–4] Earlier work carried out at our laboratories,[5] has completely dissociated the flash phenomenon from the cratering mechanism. Subsequent work reported in Ref. 6 and 7 has shown that the flash is observable at velocities well below the threshold velocities for impact explosions as described in Ref. 8. Our studies on the correspondence between the characteristics of the radiant energy emitted and the properties of the target-projectile combination, led us to place more emphasis on the study of the physical characteristics of the phenomenon in order to clearly understand the processes responsible for its generation. Experimental work has been carried out to study the time history, the spectral distribution and the intensity of the radiant energy emitted in the impact flash by means of photography, spectroscopy, and radiometry.

These experimental observations have revealed that there exist two different types of impact flash. One or both types may be present in a given impact depending mainly on the geometry of the colliding surfaces of the projectile and target. In the particular case of a spherical projectile impact, the two types of impact flash are observed consecutively such that the impact flash intensity time signature is characterized by a double pulse.

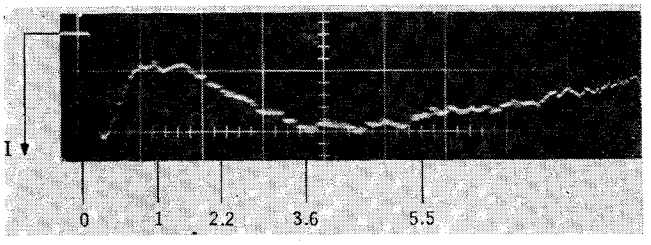

Fig. 1 Impact flash time signature. Ti-Cd impact. Sweep 1 μsec/div.

Presented as Paper 69-364 at the AIAA Hypervelocity Impact Conference, Cincinnati, Ohio, April 30–May 2, 1969; submitted May 9, 1969; revision received March 9, 1970. This work was supported in part by the Directorate of Industrial Research, Defence Research Board of Canada and partly by NASA Manned Spacecraft Center, Houston.

* Presently with the Defence Research Board of Canada.

It is the purpose of this paper to present the experimenta evidence for the dual origin of the impact flash and to give an interpretation for the mechanism which generates the observed radiation. In addition, many of the experiments employing spherical projectiles were used in a parametric investigation to determine whether the characteristics of one or both types of flash could be related to projectile characteristics, i.e., the projectile size and velocity. The results of the latter experiments are also summarized and discussed later in the paper.

II. Flash Signature

The time signature of the flash produced by the impact of a sphere on a target as measured by photodetectors reveals that two distinct phenomena appear to contribute to the generation of radiation. Two light pulses are recorded. Initially one observes a pulse with a half width of one μsec or smaller and a rise time smaller than 0.2 μsec. This initial pulse will be referred to as the "spike." It is immediately followed by a slow-rising pulse of 3–5 μsec half width. Figure 1 gives a typical example of these phenomena where the flash is produced by the impact of a 3 mm titanium sphere on a cadmium target at 3.5 km/sec. The initial pulse or spike rises to a maximum in 0.16 μsec and has a half width of 0.5 μsec. The second pulse or "tail" reaches maximum 3.4 μsec after the onset of the spike, i.e., at a time when the projectile would have travelled 7.5 times its radius into the target if it had continued unimpeded.

Open shutter photographs of the flash phenomena also reveal the presence of two zones of different intensities which

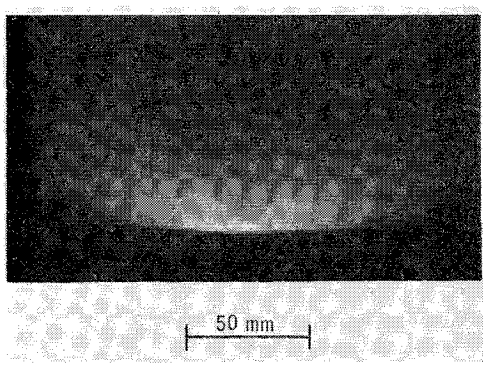

Fig. 2 Time integrated Photograph of impact flash. Ti-Cd impact.

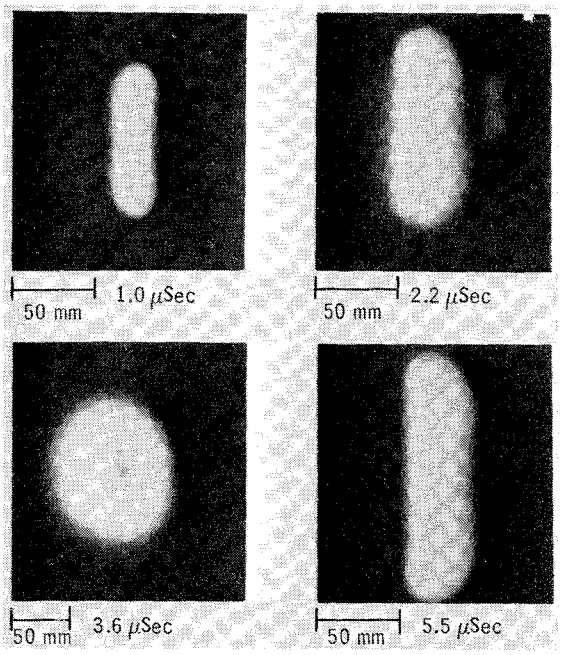

Fig. 3 Time-resolved photographs of the luminous cloud propagation. Ti-Cd impact.

would correspond to the two pulses observed in the time signature. Figure 2 shows a photograph of the impact flash for the preceding example. The two zones are well distinguished in the picture: a spot of high intensity immediately under the projectile and a diffuse luminous cloud surrounding the impact zone.

Time-resolved photographs obtained with image converter cameras triggered at preselected times have permitted us to observe the growth of the luminous cloud. The sequence of pictures shown in Fig. 3 was taken at 1.0, 2.2, 3.6, and 5.5 μsec after the start of the "spike." This clearly indicates that the "tail" of the impact flash is associated with the radiation emitted by the expanding luminous zone, which takes the shape of a well-defined luminous ring..

The observation of a luminous ring dissociates completely the tail of the impact flash pulse from the cratering mechanism, since the radiation originates from a region far removed from the impact point. Measurements of the expansion velocity of the luminous cloud may be made from the time-resolved photographs. Measurements made for impacts varied between 2 and 7 km/sec have shown that the expansion velocity is a slowly increasing function of the impact velocity. In the example just cited, the luminous zone expands at 11.6 km/sec or 3.3 times the projectile impact velocity.

The peak intensity of the radiation emitted in the luminous cloud as measured by an S-11 response photodetector varies as the fourth power of the impact velocity, all other parameters remaining fixed. This intensity measurement, however, is strongly influenced by the ambient pressure, and by the target and projectile surface finish.

Origin of the Luminous Cloud

The characteristics of the luminous cloud are most easily demonstrated by firing cone-shaped projectiles. The reason for this is that many of its properties are a function of the angle between the target surface and the projectile surface. For the case of a spherical projectile, this angle varies from 0° at the instant of impact to 90° when the projectile has penetrated a distance equal to its radius. For a conical projectile the angle is a constant.

In order to explain the origin of the luminous cloud, and thus of the tail, we list here for reference a summary of results obtained from cone firings. 1) The luminous ring disappears

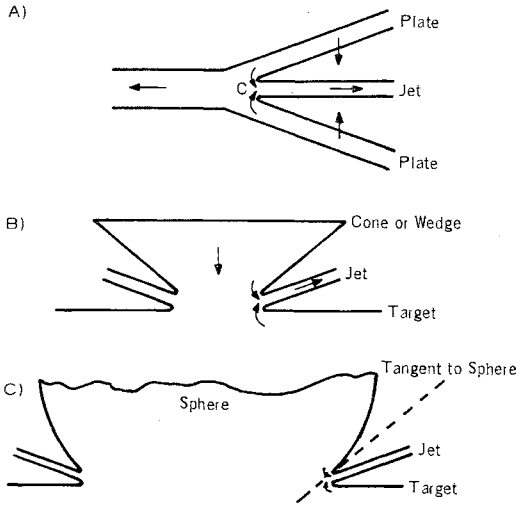

Fig. 4 Similarity of a) two plate collision to b) cone and c) sphere impact.

when the angle between the target surface and the cone surface is less than a certain critical angle α_c. The angle α_c depends on the target material, the cone material, and the cone velocity. Little or no light is detected for the impact cone whose impact angle is smaller than α_c. 2) For a given impact velocity, the luminous ring velocity decreases as the cone angle increases. The maximum ring velocity is observed at the critical angle. 3) The luminous ring produced by a cone at the critical angle travels faster than the luminous ring produced by a sphere at the same velocity.

Consideration of shaped-charge theory gives insight into the reason for these experimental observations. The collision of a cone on a flat target is analogous to the collision of two flat plates or the explosive collapse of a conical liner to which the shaped-charge theory applies. In the treatment by Taylor and Birkhoff[9] on the symmetrical collision of two plates, the generation of a jet of material is predicted whose velocity decreases with increasing angle between the two colliding plates. A similar situation exists for a cone impact on a flat plate. The same theoretical approach thus should apply to the two cases. The similarity between a cone and a flat plate impact is evident from Fig. 4.

Consider the symmetrical impact of two flat plates as depicted in Fig. 5. In a moving coordinate system which is stationary with respect to the contact point "A" between the two plates, the plates move toward that point with a velocity $|V|$. Taylor and Birkhoff argued that for a steady incompressible flow in the region of the contact point "A," the Bernouilli equation is valid such that the material in the jet and in the slug should recede from the point "A" at the same velocity $|V|$. Thus the jet velocity in the laboratory can be obtained purely from geometrical considerations. In this theory, if the impact angle between the two plates decreases toward zero, the outgoing jet velocity will tend to infinity. Experiments on jets produced by flat-plate collisions have shown that this is not the case and that there exists a minimum angle below which no jet is produced. Walsh,[10]

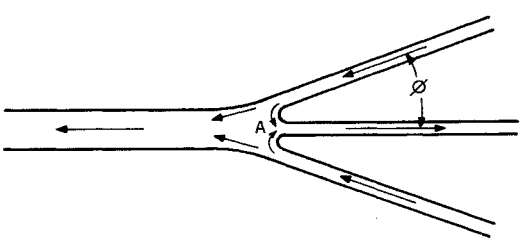

Fig. 5 Geometry of two plate collision.

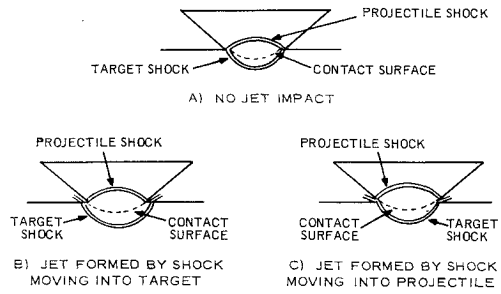

Fig. 6 Jetting due to cone impact.

in his treatment on the limiting conditions for jet formation, found that a jetless collision was indeed possible when the angle of collision was smaller than a certain critical angle. He argued that as long as the shock wave produced by the collision of the two plates remains attached at the contact point "A" the shocked material is effectively held behind the two colliding surfaces and no jetting can result. If, however, one of the shocks moves ahead of the collision point, shocked material could escape in the form of a jet.

Different configurations give rise to different jetting situations which are depicted in Fig. 6 for the asymmetrical collision of a cone on a target. Three configurations are possible. First, in Fig. 6a, the velocity of the collision point is larger than the velocity of either the target or projectile shock wave. The shock wave is then continuously attached to the collision point and the shocked material is trapped between the two shock waves, and no jetting results. The critical angle has not yet been reached. Second, in Fig. 6b, the horizontal velocity of the target shock wave may be greater than the velocity of the collision point; in that condition, shocked target material can escape in the form of a jet. Third, in Fig. 6c, a similar situation as depicted previously may exist for the projectile shock. According to these illustrations, the critical angle is that angle at which one or the other shock wave may detach from the collision point.

In jetless collisions, where the angle is smaller than the critical value, very high pressures exist in the region between the two shock surfaces. A jetless configuration for an asymmetric collision is shown in Fig. 7. The coordinate system is moving with the collision region, such that the junction of the planes containing the original surfaces of the target and projectile appears to be stationary. ρ_{01} and ρ_{02} are the densities of the projectile material and the target material. U_{01} is the velocity of the projectile material, measured in the plane of the projectile surface, and U_{02} is the velocity of the target material measured in the plane of the target surface. In the laboratory system of coordinates the target is stationary, so U_{02} is also the velocity of the coordinate system

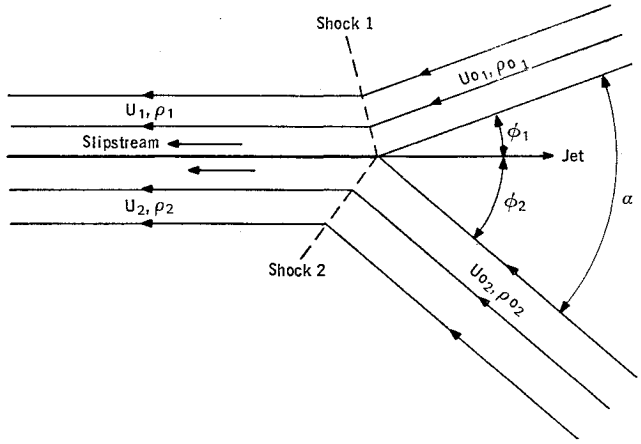

Fig. 7 Asymmetric collision as seen by an observer at rest at A.

Table 1 Comparison between the measured and derived values of the critical angle for copper-aluminum impact

Projectile velocity, km/sec	Critical angle, calculated, deg	Critical angle, measured, deg
1.0	11.2	12.5 ± 0.7
3.0	19.5	17.0 ± 2
3.5	21.5	22.0 ± 3
5.5	28.0	28.0 ± 1
6.3	29.8	32.0 ± 3

which is moving with the contact point. The pressure P must be constant across the contact surfaces (slipstream) which separates the two dissimilar systems. A breakdown of the jetless configuration must occur when either $\phi_1(p)$ or $\phi_2(p)$ reaches the critical angle associated with that stream. The critical angle is then given by

$$\alpha_c(P_c) = \phi_1(P_c) + \phi_2(P_c) \tag{1}$$

where P_c is the smaller of P_{c1} and P_{c2}. P_{c1} is the pressure associated with the maximum possible deflection of the projectile stream, and P_{c2} is the pressure associated with the maximum possible deflection of the target stream. These are referred to as critical pressures. According to Walsh the critical angle is obtained for the value of the pressure behind the shock which will satisfy the relation

$$\frac{dP}{d\mu_1} = \frac{P(P - \rho_{01}\mu_1)}{(\mu_1 + 1)[\mu_1\rho_{01}U_{01}^2 - P(\mu_1 + 2)]} \tag{2}$$

where $\mu_1 = (\rho_1/\rho_{01}) - 1$, ρ_1 is the density of the shocked projectile material, ρ_{01} is the density of the unshocked projectile material. A similar equation exists for Pc_2. The density of the shocked material can be calculated from the Rankine-Hugoniot equation

$$\rho_0 W = \rho(W - U) \tag{3}$$

where W is the shock wave velocity and U is the particle velocity behind the shock.

If the conditions are such that jetting can occur at the collision point the pressure in the shocked material has a low value. As viewed by an observer at the collision point, the collision process appears to remain unchanged in time or in other words appears as steady motion. It follows that Bernouilli's equation can be used to describe the flow.

In the laboratory coordinate system, the jet velocity is the vector sum of the jet velocity as seen by an observer at the collision point and the velocity of the collision point in the laboratory coordinate system. Figure 8 shows the projectile and target vectors and their components. The projectile jet velocity in the laboratory coordinate system is the sum of $Vo/\sin\alpha$ and $Vo/\tan\alpha$, where Vo is the projectile velocity. We obtain for the projectile velocity and the target velocity

$$U_{1j} = (Vo/\sin\alpha)\,[\cos^2\alpha + 1 + 2\cos\alpha\cos\beta]^{1/2} \tag{4}$$

Table 2 Comparison between the measured and the calculated values of the jet velocity V_j to projectile impact, velocity V_1 for Cu-Al impact

Impact angle, deg	V_j/V_1, measured	V_j/V_1, calculated
10	13.0	11.55
22	5.5	5.91
25	4.9	4.96
27	4.7	4.38
27	3.6	4.38
30	3.2	3.79
35	3.3	3.17
40	3.5	2.86

Table 3 Luminous ring and "fast" jet velocity for aluminum sphere impact on aluminum target

Projectile velocity, km/sec	Luminous ring, km/sec	Fast jet, km/sec
5.30	15.6	33.0
4.94	17.0	37.6
3.89	14.6	32.0
6.05	18.6	35.0
6.04	16.8	32.4
5.88	16.0	30.6

$$U_{2j} = (Vo/\tan\alpha)\ [2(1 + \cos\beta)]^{1/2} \qquad (5)$$

Both U_{1j} and U_{2i} decrease as α increases. The maximum jet velocity occurs at the critical angle. The experimental determination of the critical angle for onset of jetting has been made as a function of the impact velocity. Table 1 represents the results obtained compared to the theoretically-derived critical angle value. Jet velocity measurements have also been done for cone impacts at different angles of impact. The results listed in Table 2 are compared with the theoretically-calculated jet velocity.

The jet predicted by shaped-charge theory has two of the properties exhibited by the luminous ring, i.e., it disappears below a certain critical angle, and the jet velocity decreases as the cone angle increases. The above analysis has predicted the jet velocity as a function of the impact angle α, from purely geometrical considerations. The maximum velocity of the jet should occur at the critical angle whether the projectile is a cone or a sphere. Experimentally, however, a difference is measured between the jet velocity produced by a cone at the critical angle and a sphere at the same velocity. One can explain the difference by the fact that for a cone impact the angle remains constant for the whole duration of the penetration, whereas for a sphere, the impact angle sweeps from 0° to 90° passing through the critical angle at a rate which will be a function of its diameter. The amount of material thus emitted in the jet is a function of the amount of time the projectile spent in the region of the critical angle. The apparent decrease of luminous ring velocity with projectile diameter is then due to the very small amount of material travelling at the maximum speed, which is not photographically observed.

Origin of the Spike

The impact signature for a sphere impact has been found to consist of two parts, a spike and a tail. Jet theory gives a satisfactory explanation of the origin of the tail. In terms of the same jet theory the origin of the spike can be explained as follows.

In the specific case of a spherical projectile, the initial impact is normal and as time goes on the impact angle increases from 0° through to 90°. During that period the pressure behind the shock increases steadily from a value associated with normal impact to a maximum value for an oblique impact at the critical angle. At this instant there will be a detachment of the shock wave from the projectile-target impact point, and the pressure at that point will abruptly decay to a low value associated with the steady-state jetting already described. However, during this decay from high to low pressure, expansion of high energy shocked material must occur at the free surface exposed by the detached shock wave. This short-lived decay period should therefore give rise to a small amount of high-speed material travelling in advance of and at a higher speed than the steady-state jet predicted by shaped-charge theory. Such a jet, termed a "fast" jet, has in fact been observed by placing secondary targets mounted at right angles to the main target. These targets, consisting of aluminized Mylar attached to a grounded metallic plate, closed a trigger circuit when struck by ionized debris. The fast jet is not luminous for the same reason that one does not observe the maximum theoretical luminous ring velocity in the case of a sphere, i.e., too little material is involved.

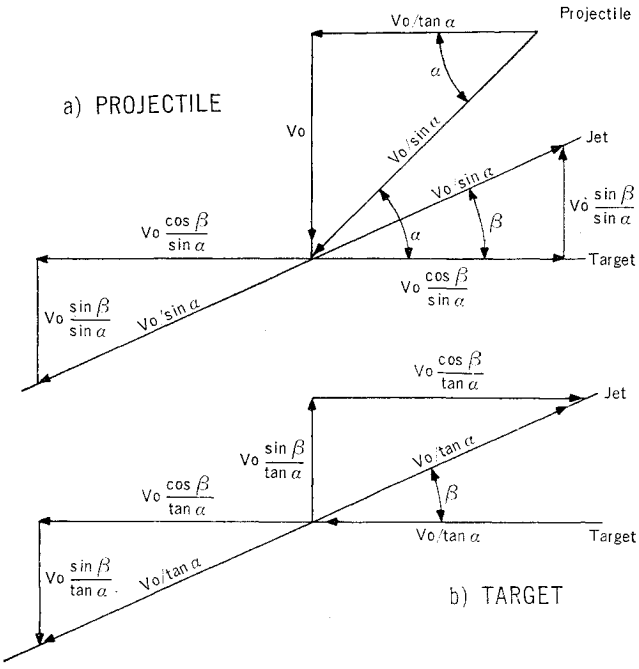

Fig. 8 Target and projectile velocity vectors and components.

Table 3 shows the results obtained in the measurement of luminous ring velocity and fast jet velocity for aluminum spheres impacting on aluminum targets. In some cases involving copper sphere impacts, fast jet velocities as high as 50 km/sec have been measured. The initial luminosity of the fast jet near the contact point in the high-pressure region is apparently responsible for the spike. This also ties in with the spectroscopic analysis of the impact flash as discussed later.

III. Spectroscopic Studies

The time and space-integrated radiant energy generated by hypervelocity impact was spectroscopically examined from the near infrared to the ultraviolet region of the electromagnetic spectrum. Figure 9 presents a typical spectral distribution of the radiant energy emitted by the flash. The experiment consisted in colliding a 6.4 mm aluminum sphere against a cadmium target at 7 km/sec in a range maintained at a pressure of 5×10^{-5} Torr. The spectrum is recorded on a uv sensitive plate by means of a f/6.8 Czerney Turner mount spectrograph viewing the flash phenomenon normal to the line of flight of the projectile. All spectra thus obtained

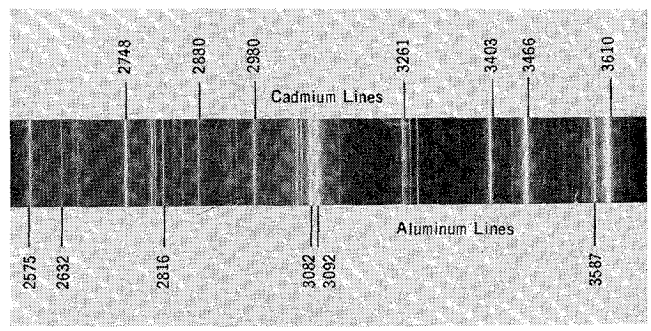

Fig. 9 Space-integrated spectrum of the impact flash. Al-Cd at 7 km/sec.

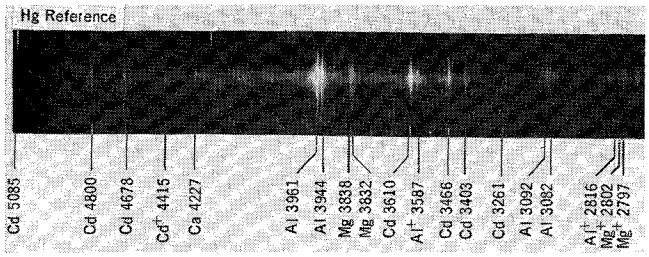

Fig. 10 Space-resolved spectrum. Al-Cd impact at 5 km/sec.

were of the line emission type, from which one can identify many lines pertaining to transition of the neutral atoms of both target and projectile material. The spectra also generally revealed the presence of many transitions of the ionized species of the same elements. No band emission or line emission of the ambient atmosphere was observed. Finally a background continuum remains undetected in this type of spectral record, due to its low spectral radiance in the impact flash dispersed over a wide wavelength region. These results allow us to conclude that the impact flash is caused by radiant energy produced by a gas at high temperature.

In order to have a better insight into the phenomenon, the impact flash region was focussed on the entrance slit of the astigmatic spectrograph viewing normal to the projectile line of flight in the plane of the target. A space resolved spectrum of the impact flash is thus recorded. Figures 10 and 11 show the space-resolved spectrum of the impact flash produced by the collision of an aluminum sphere on a cadmium target at 7.0 km/sec and of aluminum on aluminum at 6 km/sec. The spectrograms reveal the presence of two clearly distinguishable zones which would correspond to gas in two different thermodynamic states. The spectrum clearly differs from the space-integrated spectrum in that there is now an important continuum in the region of space which would correspond to the impact zone. This zone contains lines of high excitation transition of atoms or ions, whereas in the surrounding zone, which would be related to the luminous cloud, one observes the most sensitive emission lines of a gas at an arc temperature. Two different gaseous states are thus also detected spectroscopically. The observed continuum is predominant in the wavelength region corresponding to the most sensitive lines of aluminum and cadmium atoms in the near ultraviolet region. This would rule out the shocked surface of projectile or target as the source of continuum gray-body radiator. The type of continuum recorded corresponds to a resonance broadening normally observed from a radiating gas at high pressure. The resonance broadening mainly affects excited states having a large degeneracy.

The broadening exists only at the impact point. Away from it, along the path of the luminous ring, little or no broadening is observed. A space-resolved spectrum is in some respects also time resolved since points on the film which are successively farther away from the impact point are

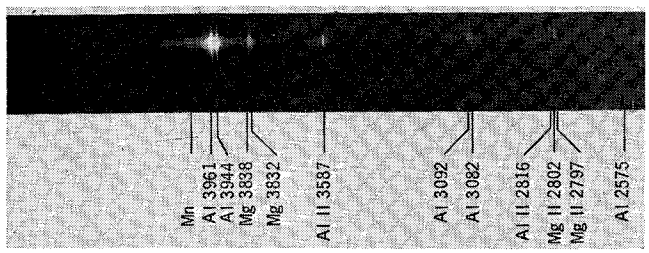

Fig. 11 Space-resolved spectrum. Al-Al impact at 6 km/sec.

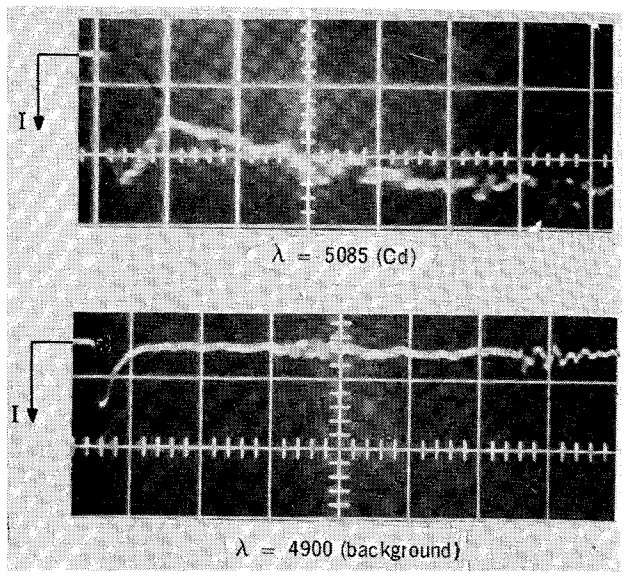

Fig. 12 Comparison between time signature for line and continuum emission. Cu-Cd impact at 5 km/sec. Sweep 0.5 μsec/div.

exposed at successively later instants of time. The broadened central portion of the spectrum and high-temperature environment correspond to the spike, and the relatively sharp emission of persistent lines which extend on either side of the impact point corresponds to the tail. This experiment provides evidence that the spike is produced in a region of high pressure which, as explained earlier, leads to the formation of the fast jet.

Further evidence of this effect has been obtained from time-resolved spectroscopy. These observations were made by mounting four photomultiplier heads in the focal plane of the spectrograph and setting them at positions behind exit slits fixed at preselected wavelengths.

Figure 12 shows the traces from two photomultipliers monitoring one line of a cadmium atom transition at 5085 Å and a background band in the same region (4900 Å), which does not correspond to any line of the elements involved in the process. The correspondence between the space and time resolved spectrum is well marked here. The 5085 Å transition is presented in both spike and tail, whereas the 4900 Å band is recorded only during the early phase of impact giving rise to the spike only.

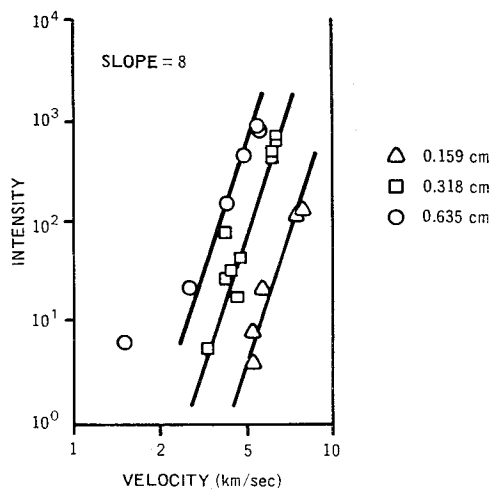

Fig. 13 Spike peak intensity of the 3610Å transition vs projectile velocity.

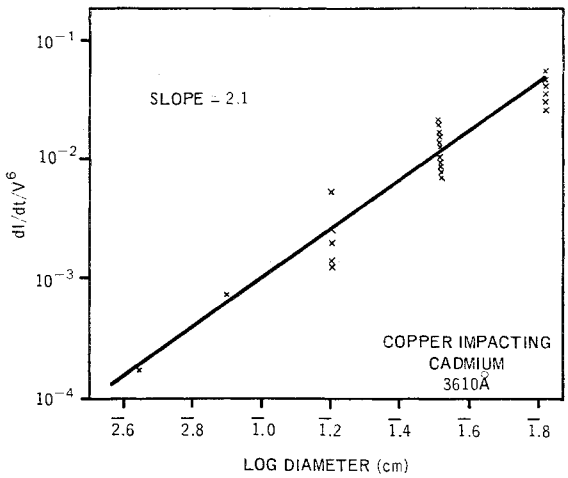

Fig. 14 Normalized spike intensity vs projectile diameter.

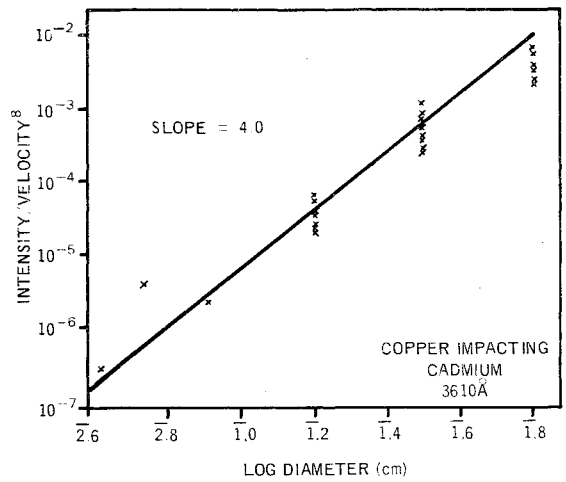

Fig. 16 Normalized rate of change of intensity vs projectile diameter.

IV. Parametric Studies

The impact flash signature has also been investigated to determine if any of its characteristics are capable of providing quantitative information about the size and velocity of the projectile. Parametric experiments have been made in which the diameter and velocity of copper spheres, impacting cadmium targets, were varied in the ranges 1.6 mm to 6.4 mm, and 2.0 km/sec to 8.0 km/sec respectively. As mentioned earlier sphere impacts have an impact flash emission line signature which consists of a spike and a tail. In these parametric studies only the spike has been considered as a good observable, the tail presenting data which exhibited considerable scatter. The experiments were conducted by means of a direct reading spectrograph with three photomultipliers monitoring three different narrow wavelength bands of the flash emission spectrum. The bandwidths were 20 Å, and the three wavelengths monitored were three emission lines of cadmium at 5085 Å, 3610 Å, and 3261 Å.

It was found that the peak intensity (I) and the initial rate of change of intensity (dI/dt) of the spike, for chosen emission lines of cadmium, were strongly and consistently dependent on the diameter and velocity of the projectile. The peak intensity of the spike varies as the eighth power of the projectile velocity for all three of the cadmium lines analyzed. Figure 13 shows the variation of the peak intensity of the 3610 Å line as a function of the velocity for copper spherical projectiles of different diameters. To find the dependence on diameter, the measured intensities were normalized by dividing by the impact velocity taken to the power of eight. Figure 14 shows the variation of I/V^8 with projectile diameter for the 3610 Å cadmium line in copper impact. For all the lines observed, the intensity appears to vary as d^3 to d^4 depending on the emission lines studied.

The rate of change of spike intensity dI/dt also depends on the properties of the impacting projectile. The rate of change of spike intensity varies as to the sixth power of the projectile velocity and is also a function of the projectile diameter. Figure 15 shows the variation of dI/dt with velocity for the 3610 Å transition of cadmium and Fig. 16 shows the dI/dt divided by V^6 dependence with the projectile diameter. The rate of change of intensity appeared to vary as d^2 approximately for the emission lines studied.

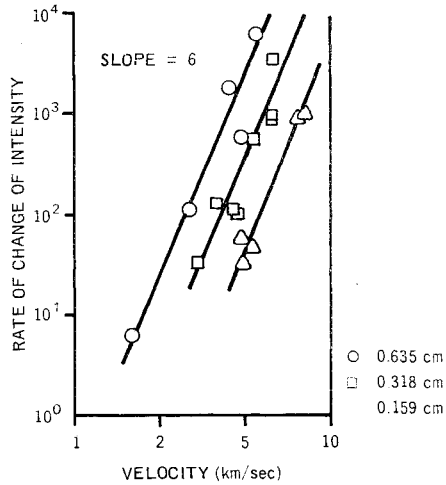

Fig. 15 Rate of change of intensity of the 3610Å transition vs projectile velocity.

V. Conclusion

The impact flash that is usually observed to be generated by a projectile impact at hypervelocity has been explained in terms of the mechanism of the shock wave propagation in both projectile and target, and the geometry of the colliding surfaces of the projectile and target. It has been demonstrated that one of the observed time-resolved phenomena, the short duration transient spike, can be attributed to the presence of a hot, dense plasma at the impact point, whereas the slow-rising, long-duration tail is due to the radiation of a neutral gas expanding from the impact zone.

Jets of particles have been observed to be associated with each of the two radiation sources; for the spike a fast jet of nonradiating particles, for the tail a luminous jet. The latter has been explained by analogy with the shaped-charge theory developed for collapsing liners. Its velocity and behavior as a function of projectile geometry has been correctly predicted. The origin of the former, however, is somewhat speculative since its characteristics have not been quantitatively evaluated, although it is considered that a plausible explanation has been offered. Further work on this subject would be fruitful.

References

[1] Clark, J. S., Kodesch, R. R., and Grow, R. S., "Spectral Analysis of the Impact of Ultra Velocity Copper Spheres into Copper Targets," TR OSR 13, Sept. 1959, Univ. of Utah, Salt Lake City, Utah.

[2] MacCormack, R. W., "Investigation of Impact Flash at Low Ambient Pressure," *Proceedings of the Sixth Symposium on Hypervelocity Impact*, The Firestone Tire and Rubber Co., Cleveland, Ohio, Vol. II, Pt. 2, 1963, pp. 613–625.

[3] Gehring, J. W. and Warnica, R. L., "An Investigation of the Phenomena of Impact Flash and its Potential Use as a Hit Detection and Target Discrimination Technique," *Proceedings of the Sixth Symposium on Hypervelocity Impact*, The Firestone Tire and Rubber Co., Cleveland, Ohio, Vol. II, Pt. 2, 1963, pp. 627–681.

[4] Koehler, R. A., "Spectroscopic Study of the Impact Flash," M.S. thesis, 1965, Univ. of Western Ontario, London, Ontario, Canada.

[5] Jean, B., "Experimental Observations of Optical Radiation Associated with Hypervelocity Impact," *AIAA Journal*, Vol. 4, No. 10, Oct. 1966, pp. 1854–1856.

[6] Rollins, T. L. and Jean, B., "Impact Flash for Micrometeoroid Detection," CR-92122, May 1968, NASA.

[7] Jean, B. and Rollins, T. L., "Hypervelocity Impact Flash for Hit Detection and Damage Assessment," AFATL-TR-68-46, March 1968, U.S. Air Force, Eglin Air Force Base, Fla.

[8] Cook, A. M., "The Science of High Explosives," Reinhold, New York, 1959, pp. 259–262.

[9] Birkhoff, G. et al., "Explosives with Lined Cav ties," *Journal of Applied Physics*, Vol. 19, No. 6, June 1948, pp. 563–582.

[10] Walsh, J. M., Shreffler, R. G., and Willig, F. J., "Limiting Conditions for Jet Formation in High Velocity Collisions," *Journal of Applied Physics*, Vol. 24, No. 3, March 1963, pp. 349–359.

OCTOBER 1970 AIAA JOURNAL VOL. 8, NO. 10

Convective Electric Arcs at Mach Numbers up to 6.5

CHARLES E. BOND* AND DWIGHT N. WICKERSHEIM†
University of Illinois, Urbana, Ill.

Experimental observations are presented of supersonic convective electric arcs magnetically stabilized in sulfur hexafluoride. It is found that the arc column, moving at Mach numbers from 1.3 to 6.5, slants across the electric field lines at angles such that the crossflow Mach number ranges from 0.8 to 3.8. The experimental apparatus was a rail accelerator with one rail, usually the cathode rail, preheated to enhance arc stability. Observed values for the angle of slant are presented for three different preheat temperatures. The direction of slant was always such that the arc root at the heated rail led the remainder of the arc. At Mach numbers above 2.0 and preheat temperatures T_R of 1700°C and 2200°C, the magnitude of the slant angle was given very nearly by $\cos^{-1}(T_1/T_R)^{1/2}$, where T_1 is the temperature of the gas ahead of the arc. For the preheat temperature of 1100°C, the slant angle has a maximum which is also given by $\cos^{-1}(T_1/T_R)^{1/2}$. Observations of the effective drag coefficient for the arc column are presented and discussed.

Introduction

FOR the convective electric arc in air, there exists a stable geometric configuration in which the plasma column slants across the electric field lines.[1–5] The connection between column slanting and arc stability was first discovered for the stationary blown arc in a supersonic wind tunnel,[1,2] and later confirmed for the moving arc in a thermionic rail accelerator.[5] It has been shown that the stable supersonic arc in air slants very nearly along a Mach line—i.e., the component of velocity normal to the arc column is approximately equal to the speed of sound in the undisturbed gas.

Experiments are discussed herein in which electric arcs moving through sulfur hexafluoride were observed. These arcs also slanted across the electric field lines, but at angles such that the normal component of velocity ranged from about 0.8 to 3.8 times the speed of sound in the undisturbed gas.‡

Received August 1, 1969; revision received December 11, 1969. This work was sponsored by Project SQUID, which is supported by the Office of Naval Research, Department of the Navy, under Contract N00014-67-A-0226-0005, NR-098-038. Reproduction in full or in part is permitted for any use of the U.S. Government. The authors gratefully acknowledge the assistance of R. W. Potillo, L. M. Corley, R. Weber, R. Fiscus, D. Heim, and T. E. Schulze.

* Associate Professor, Department of Aeronautical and Astronautical Engineering.

† Research Assistant, Department of Aeronautical and Astronautical Engineering; now Thermodynamic Engineer, Lockheed Missiles & Space Company, Sunnyvale, Calif.

‡ A further paper[6] is now in publication which reports a fine sawtooth structure for the arc column in SF_6, and indicates that the column mechanism tending to produce a crossflow Mach number of unity is locally effective in SF_6.

The experiments were conducted in a thermionic rail accelerator, in which the electric arc is established between parallel rail electrodes in a stationary gas and accelerated to equilibrium speed by a uniform impressed magnetic field normal to the electrode plane. The cathode rail was preheated to enhance thermionic emission and minimize the destabilizing influence of arc root phenomena.[1] Sulfur hexafluoride was used for the present experiments primarily because its low speed of sound permits observation of arcs at high Mach numbers by means of conventional high-speed photographic procedures.

Side-view photographic observations showed that the magnitude of the angle of slant increased with cathode rail temperature. For the highest rail temperature employed (2200°C), the arc column approached the Mach slant and was most stable and straight. Stable convective columns of considerable length were observed, the length-to-width ratio ranging up to about 50.

Head-on observations showed 1) that in the stable mode, the convective arc column in SF_6 remains remarkably straight and in the plane of the electrodes, 2) that the luminosity width of the stable arc column (measured normal to the electrode plane) is greater than the arc thickness,§ 3) that the column width does not vary appreciably along the length of the stable supersonic column as it does for the low-subsonic column in nitrogen[4] and 4) that in the unstable mode, the arc column fluctuates out of the electrode plane.

Highly unstable arcs were obtained when both electrodes were unheated. Column stability was greatest with a heated

§ Reference 7 reported a similar cross-sectional shape for arcs in air at crossflow Mach numbers around 0.05, as did Ref. 3 for crossflow Mach numbers around 1.0. See also Ref. 8.